LM-06K125
November 3, 2006

SCC Initiation in Alloy 600 Heat Affected Zones Exposed to High Temperature Water

E Richey, DS Morton, RA Etien, GA Young and RB Bucinell

NOTICE

SCC INITIATION IN ALLOY 600 HEAT AFFECTED ZONES EXPOSED TO HIGH TEMPERATURE WATER

Edward Richey, David S. Morton, Robert A. Etien, George A. Young
Lockheed Martin
2401 River Road
Schenectady, NY 12309

Ronald B. Bucinell
Union College, Department of Mechanical Engineering
Steinmetz Hall
Schenectady, NY 12308

ABSTRACT

Studies have shown that grain boundary chromium carbides improve the stress corrosion cracking (SCC) resistance of nickel based alloys exposed to high temperature, high purity water. However, thermal cycles from welding can significantly alter the microstructure of the base material near the fusion line. In particular, the heat of welding can solutionize grain boundary carbides and produce locally high residual stresses and strains, reducing the SCC resistance of the Alloy 600 type material in the heat affected zone (HAZ). Testing has shown that the SCC growth rate in Alloy 600 heat affected zone samples can be ~ 30x faster than observed in the Alloy 600 base material under identical testing conditions due to fewer intergranular chromium rich carbides and increased plastic strain in the HAZ [1, 2]. Stress corrosion crack initiation tests were conducted on Alloy 600 HAZ samples at 360°C in hydrogenated, deaerated water to determine if these microstructural differences significantly affect the SCC initiation resistance of Alloy 600 heat affected zones compared to the Alloy 600 base material. Alloy 600 to EN82H to Alloy 600 heat-affected-zone (HAZ) specimens where fabricated from an Alloy 600 to Alloy 600 narrow groove weld with EN82H filler metal. The approximate middle third of the specimen gauge region was EN82H such that each specimen had two HAZ regions. Tests were conducted with in-situ monitored smooth tensile specimens under a constant load, and a direct current electric potential drop was used for in-situ detection of SCC. Test results suggest that the SCC initiation resistance of Alloy 600 and its weld metal follows the following order: EN82H > Alloy 600 HAZ > Alloy 600. The high SCC initiation resistance observed to date in Alloy 600 heat affected zones compared to wrought Alloy 600 is unexpected based on the microstructure of HAZ versus wrought material and based on prior SCC growth rate studies. The observed behavior for the HAZ specimens is likely not related to differences in the environment, differences in surface stress/strain between the various specimen regions(weld, HAZ, wrought), differences in surface residual stress, or differences in the microstructure of the various specimen regions (weld, HAZ, wrought). The behavior may be related to differences in the creep behavior of the various weld regions or differences in the surface area of the various materials (weld, HAZ, wrought) exposed to high temperature water.

Keywords: stress corrosion cracking, SCC, initiation, Alloy 600, heat affected zone

INTRODUCTION

Nickel-chromium-iron alloys exhibit intergranular stress corrosion cracking (SCC) at temperatures greater than ~250°C when exposed to high purity water. Studies have shown that grain boundary chromium carbides improve the SCC resistance of nickel based alloys exposed to high temperature, high purity water [3-9]. However, thermal cycles from fusion welding can solutionize beneficial grain boundary carbides, produce locally high residual stresses and strains, and promote SCC in the heat affected zone (HAZ). Studies have shown that SCC growth rates in Alloy 600 heat affected zones are ~30X faster than the Alloy 600 base material under the same test conditions [1, 2]. The increased crack growth rate of the Alloy 600 HAZ relative to the base metal was attributed to fewer intergranular chromium rich carbides and to increased plastic strain in the HAZ.

Degradation by SCC involves both an initiation phase and a crack growth phase. Although extensive studies have been performed to characterize the effects of key parameters on SCC growth (*e.g.* temperature, stress intensity factor, etc.), limited studies have been performed to examine SCC initiation. The present work summarizes efforts to quantify the SCC initiation time of Alloy 600 HAZ samples in high temperature water. Stress corrosion crack initiation tests were conducted on Alloy 600 HAZ samples at 360°C in hydrogenated, deaerated water to determine if these microstructural differences significantly affect the SCC initiation resistance of Alloy 600 heat affected zones compared to the Alloy 600 base material.

EXPERIMENTAL

Material

Alloy 600 to EN82H to Alloy 600 heat affected zone specimens were fabricated from an Alloy 600 to Alloy 600 narrow groove weld with EN82H filler metal. The Alloy 600 was in the mill annealed condition (final anneal at 982°C). This narrow groove weld geometry has been described previously [10]. The narrow groove weld was made using cold-wire automatic gas tungsten arc welding (CW AGTAW) with a 100% Ar cover gas. The Alloy 600 and EN82H heats were NX5805G and XY491, respectively. Table 1 contains the chemical compositions and available tensile properties for these heats. The test specimens were button-head tensile specimens, machined according to the sketch shown in Figure 1. The approximate middle third of the specimen gauge region was EN82H such that each specimen had two HAZ regions as depicted in Figure 1. The microstructure is shown in Figure 2.

Environment

All testing was performed in hydrogenated, deaerated water at 360°C and hydrogen contents between 1 and 75 cc/kg. The autoclave pressure was maintained at 20.7 MPa (3000 psig) to preclude boiling. The feed tank solution was buffered to a room temperature pH of 10.1 to maintain a near neutral autoclave pH at the test temperature. The desired hydrogen concentration was obtained by varying the feed tank hydrogen overpressure according to Henry's law. A room temperature Henry's law coefficient of 5.9 kPa/(cc/kg) or 0.85 psia/(cc/kg) was employed. Cylinders of mixed gas containing 4% or 14.7% hydrogen, with the balance argon, were used to obtain hydrogen levels less than 20 cc H_2/kg H_2O. Pure nitrogen gas was employed to obtain test conditions with very low hydrogen levels. Since the autoclave turnover rate is relatively rapid (once every hour), autoclave effluent dissolved gas levels are analogous to feed tank levels, and the oxygen levels for all tests were <10 ppb.

Trends in pH and contaminant levels were monitored through system in-line conductivity probes. Anion contaminant levels were verified as less than detectable (~25 ppb) by ion chromatography (IC) analysis of autoclave effluent samples. Autoclave cation contaminants were monitored through analysis of autoclave effluent samples by inductively coupled plasma (ICP) spectroscopy. Cation contaminant levels typically coincided with their solubility limits (*e.g.*, ~ 2 ppb Fe) at temperature.

Table 1a: Chemical Composition (wt%)

Alloy 600 Heat NX5805G (1)		EN82H Heat XY491 (2)	
Ni	75.77	Ni+Co	70.87
Cr	15.04	Cr	20.42
Fe	7.87	Fe	2.69
C	0.07	C	0.030
Mn	0.22	Mn	2.89
Si	0.21	Si	0.09
P	0.007	P	0.002
S	0.001	S	0.003
Co	0.04	Cu	0.007
Cu	0.20	Si	0.09
Al	0.21	Ti	0.36
Ti	0.35	Nb+Ta	2.20
B	0.004	Pb	0.002
Mg	0.01	Al	-
Mo	-	Mo	-

Table 1b: Tensile Properties for Alloy 600 Heat NX5805G (3)

Temperature (°F)	σ_{YS} (ksi)	σ_{UTS} (ksi)
Room Temperature	50.2	102.7
300	47.7	94.5
600	40.9	93.8
680	31.8	90.9

NOTES:
(1) Final anneal at 1800°F.
(2) Cold wire automatic gas tungsten arc weld with 100%Ar shield gas, as-welded condition.
(3) Tensile tests performed according to ASTM E 8, σ_{YS} = 0.2% yield strength, σ_{UTS} = ultimate tensile strength.

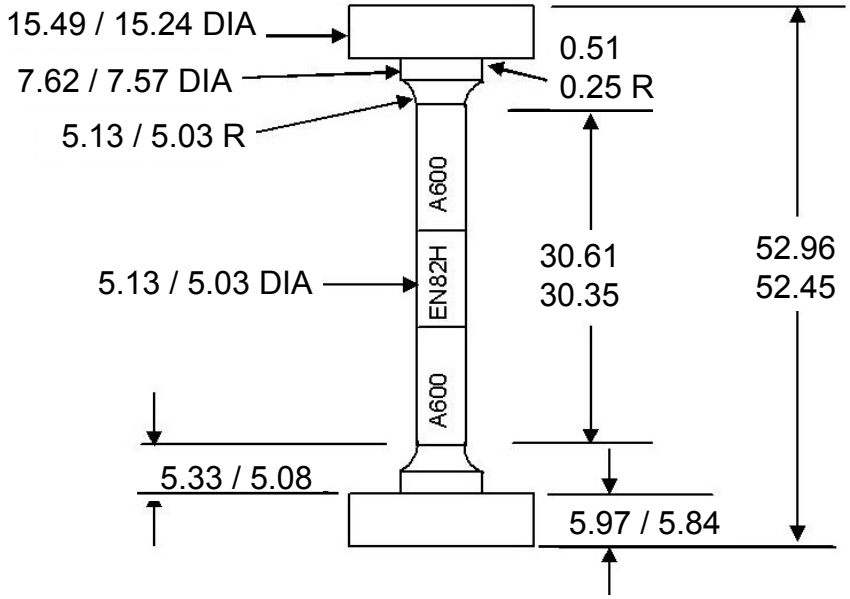

Figure 1: Schematic showing an Alloy 600-EN82H-Alloy 600 HAZ specimen. All dimensions are in mm.

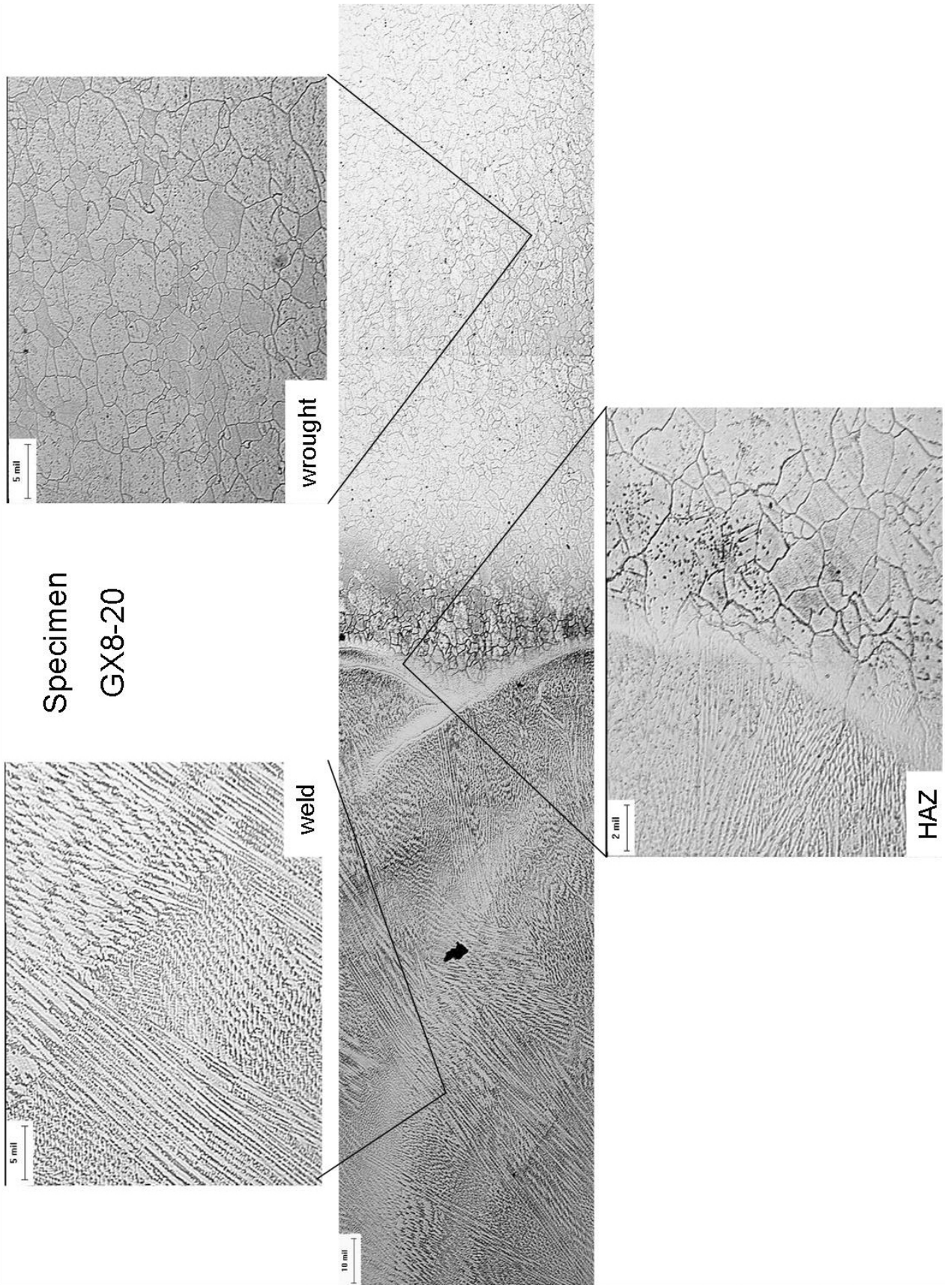

Figure 2: Optical micrographs showing the microstructure of the various weld regions in the Alloy 600 HAZ specimens.

In-situ Monitoring

All tests were instrumented with reversing direct current electric potential drop (EPD). Figure 3 shows the EPD wiring schematic. A constant DC current (I) is passed through the specimen and the voltage drop, ΔV, between probes on each end of the gauge length is measured. The current distribution is uniform, thus the voltage difference between the two probes is proportional to the distance between the probes and inversely proportional to the cross-sectional area of the gauge region. The resistance of the material is related to the gauge length and cross-sectional area as follows:

$$R = \frac{\Delta V}{I} = \frac{\rho L}{A} \tag{1}$$

where R is the resistance, ρ is the resistivity, L is the gauge length, and A is the cross sectional area. Plastic deformation is a constant volume process, thus the volume, V_o, can be related to the cross sectional area as:

$$A = \frac{V_o}{L} \tag{2}$$

As the sample is strained, the gauge length increases, and the gauge length can be expressed as:

$$L = L_o + \Delta L \tag{3}$$

where L_o is the original length and ΔL is the change in length. Combining Equations 1-3 and recognizing that $\Delta L/L_o$ is the engineering strain, the change in resistance of the sample can be related to the engineering strain, ε, as follows:

$$\varepsilon = \left(\frac{R}{R_o}\right)^{1/2} - 1 \tag{4}$$

where R_o is the original resistance of the sample $\left(R_o = \rho L_o^2 / V_o\right)$, and R is the resistance for each subsequent point. Formation of SCC reduces the gauge cross-sectional area and causes an increase in the voltage difference between the two probes. This increase in voltage signifies SCC initiation. The voltage measured on the test specimen is normalized for temperature and material resistivity changes with a voltage measured from a "reference" specimen of the same material. The "reference" specimen is pre-strained at the test temperature to the same load as the test specimen prior to testing, but it is not under any load during the test. SCC has not occurred in any of these non-loaded pre-strained specimens.

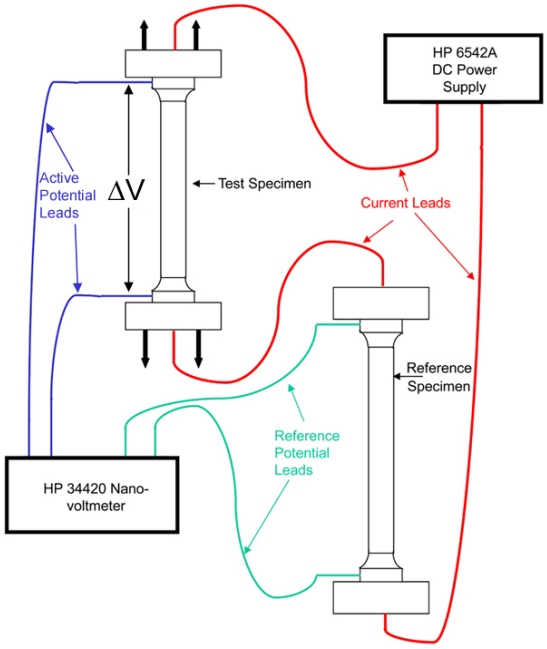

Figure 3: Schematic of the reversing direct current electric potential drop in-situ monitoring technique.

In tests where SCC occurred, a change in the slope of the EPD versus time signal was present, as illustrated in Figure 4. As shown, lines were drawn over ranges of EPD data both before and after the slope of the EPD versus time data was noted to change. The intersection of these lines was defined as the time at which SCC initiated. Slope changes have not been observed in the EPD data for tests where SCC did not occur.

Post-Test Evaluation

All specimens were visually inspected with a stereo-microscope at the end of testing to characterize the number of SCC cracks in the gauge section of the specimens. The specimens that did not fail were then tensile pulled ~1.3 mm and inspected a second time with a stereo-microscope to characterize the extent of SCC. For the specimens that failed during the test, the maximum SCC depth on the fracture surface was recorded.

RESULTS

Effect of Loading History

For the first five HAZ specimens tested, post test stereo-microscope inspections revealed that numerous intergranular cracks were present in the Alloy 600 regions of the specimens. However, SCC was not observed in either the EN82H weld metal or the EN82H to Alloy 600 heat affected zones in any of these specimens. Since SCC occurred only within Alloy 600 regions, the SCC initiation time data obtained with these HAZ test specimens actually represented wrought Alloy 600 behavior.

For the next two tests, the specimens tested were samples that had been used as EPD reference specimens during prior tests. In contrast to previous HAZ specimen results, post test stereo-microscope inspections revealed that SCC occurred in the HAZ regions of these samples. The fact that cracking occurred in the HAZ regions in these test is likely due to the loading history of the specimens. The sixth specimen tested was subjected to the following temperature/loading conditions:

1. Pre-strained to 11.0 kN (2481 lbs) at 360°C in air.
2. Tested as an EPD reference specimen in a HAZ test of specimen GX8-29 at 360°C and 30 cc/kg H_2 for 892 hours.
3. Utilized as a test specimen in a subsequent test at 360°C and 33 cc/kg H_2 for 1350 hours at 11.1 kN (2500 lbs).

The seventh specimen was subjected to the following temperature/loading conditions:

1. Pre-strained to 9.7 kN (2184 lbs) at 338°C in air.
2. Tested as an EPD reference specimen in a HAZ test of specimen GX8-21 at 360°C and 30 cc/kg H_2 for 1011 hours and as the EPD reference specimen in the HAZ test of specimen GX8-28 at 360°C, 33 cc/kg H_2 for 1350 hours.
3. Utilized as a test specimen in a subsequent test at 360°C and 33 cc/kg H_2 for 5299 hours at 11.1 kN (2500 lbs).

In Reference [11] is was hypothesized that pre-straining the specimens to a slightly lower load initially resulted in work hardening of the EN82H and Alloy 600 regions to different degrees which would result in the yield strength of the materials likely being similar after the initial loading. In the subsequent tests, the EN82H and Alloy 600 regions were strained to similar levels. As a result, microstructural differences were more important than differences in strain, thus the HAZ (which microstructurally should be more susceptible) cracked. This hypothesis was tested as detailed in the ‘Discussion’ section.

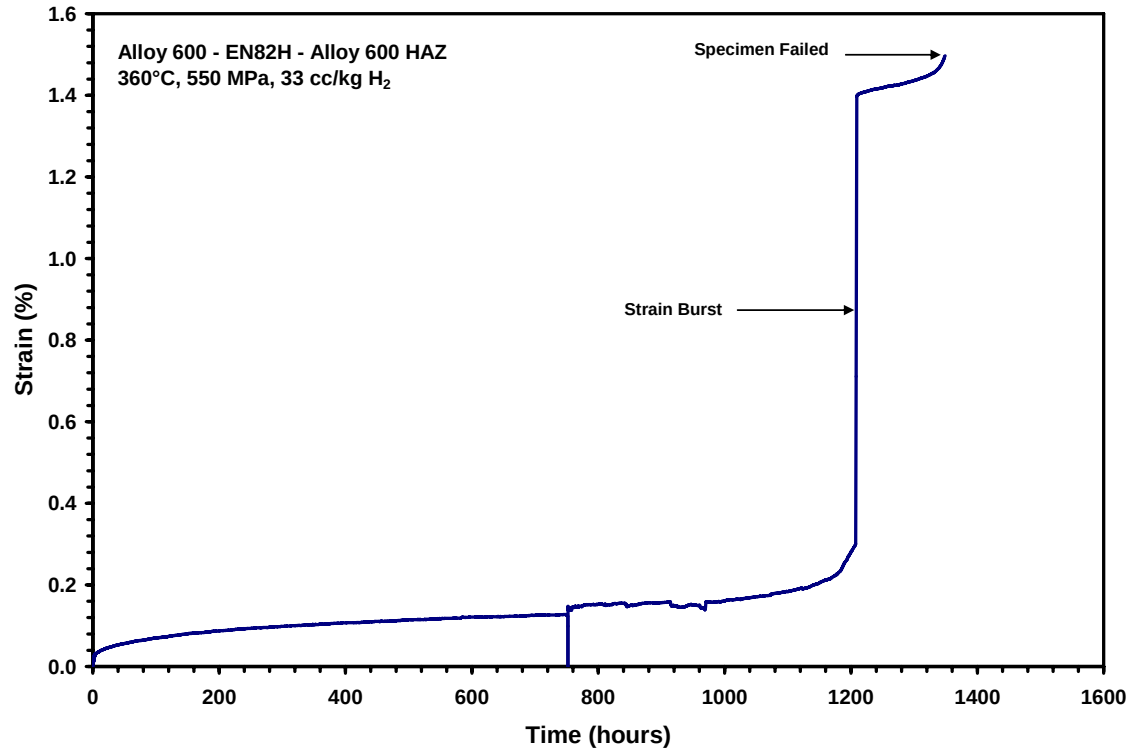

(a)

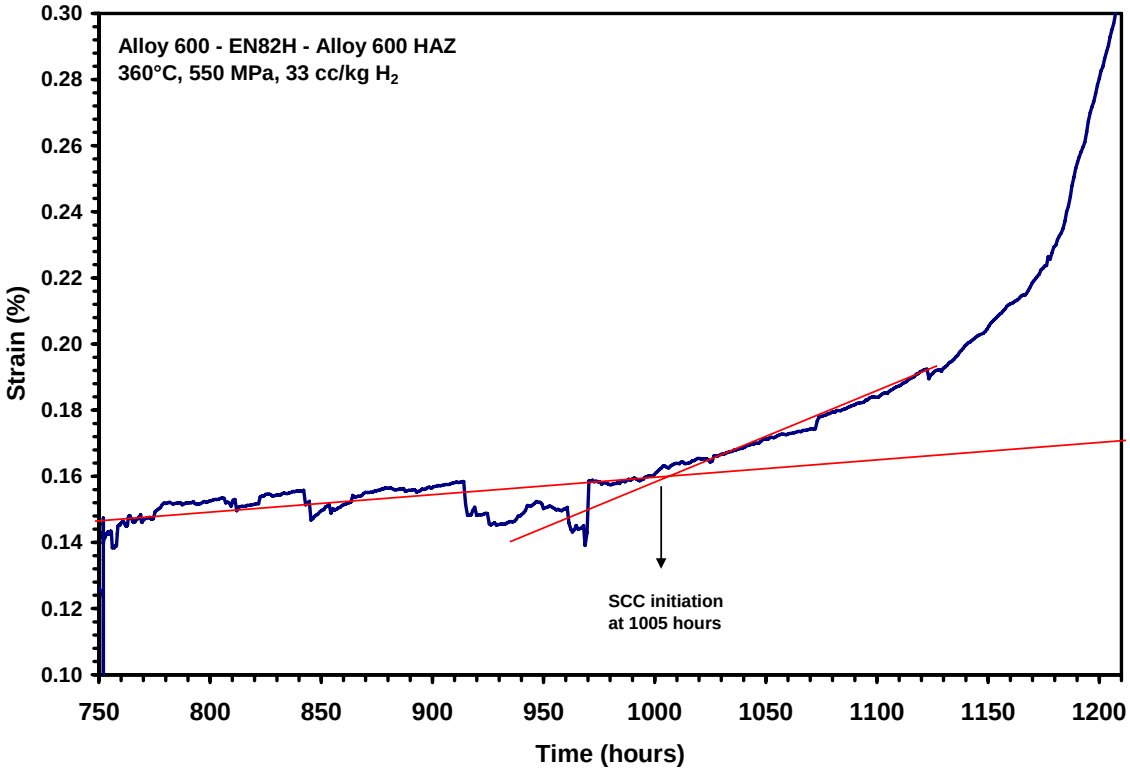

(b)

Figure 4: (a) EPD data for a test of Alloy 600 heat affected zone material (Specimen GX8-28): 360°C, 550 MPa, and 33 cc/kg H_2. (b) EPD data for a test of Alloy 600 heat affected zone material (Specimen GX8-28) illustrating EPD indicated crack initiation.

Table 2: Alloy 600-EN82H-Alloy 600 HAZ Specimens Test Results

Specimen ID	GX8-21 (5)	GX8-23 (5)	GX8-25 (5)	GX8-29 (5)	GX8-30 (5)	GX8-28 (6)	GX8-22 (6)
Material (1)	HAZ	HAZ	HAZ	HAZ	HAZ	HAZ	HAZ
A600 Heat	NX5805G	NX5805G	NX5805	NX5805	NX5805G	NX5805G	NX5805G
EN82H Heat	XY491	XY491	XY491	XY491	XY491	XY491	XY491
Condition	as welded	as welded	as welded	as welded	as welded	as welded	as welded
Surface Finish (2)	SPT	SPT	SPT	SPT	SPT	SPT	SPT
Gage Diameter (mm)	5.08	5.08	5.11	5.11	5.08	5.08	5.08
Gage Length (mm)	30.48	30.48	30.48	30.48	30.48	30.48	30.48
Temperature (°C)	360	360	360	360	361	361	361
Pressure (MPa)	20.685	20.685	20.685	20.685	20.685	20.685	20.685
Chemistry	DPW	DPW	DPW	DPW	DPW	DPW	DPW
Hydrogen (cc/kg)	30	75	75	30	1	33	1
ΔEcP (mV) (3)	1.4	26.4	26.4	1.4	-91 (8)	0.3	-102
Loading History (4)	Hot-load	Hot-load	Hot-load	Hot-load	Hot-load	Hot-load	Hot-load
Engineering Stress (MPa)	549	499	549	549	549	549	549
Engineering Strain (%)	NA	NA	NA	17.60%	15.1	7.3	16.2
Number of Strain Bursts	1	2	1	1	0	1	1
Time-to-Initiation (hrs)	520	1580	1730	NA (7)	3600	1005	4488
Total Test Time (hrs)	1011	2037	2299	890	4983	1350	5299
SCC Initiation/Failure	Yes / No	Yes / Yes	Yes / Yes	Yes / No	Yes / No	Yes / Yes	Yes / No
Crack Shape	Thumbnail	Thumbnail	Thumbnail	NA	NA	Thumbnail	NA
Max. Crack Depth (mm)	NA	1.68	1.35	NA	NA	1.27	NA
# Surface Cracks Pre-Tensile Pull	NA	NA	NA	NA	~30 (9)	~10 (10)	~4 (11)
# Surface Cracks Post-Tensile Pull	NA	NA	NA	NA	NA	NA	NA

NOTES:

(1) A600 to EN82H to A600 heat affected zone specimen.

(2) SPT = single point turn.

(3) Corrosion potential distance from the nickel oxide phase transition $\Delta EcP = (EcP_{Ni/NiO} - EcP)$. This quantity describes, fundamentally, the coolant hydrogen crack growth rate functionality [12-16]. Selected values were corrected for deviations from hydrogen electrode behavior by specimen to Platinum EcP measurements.

(4) Hot-loaded: autoclave heated to test temperature prior to loading specimen.

(5) SCC occurred only in wrought Alloy 600 specimen region (i.e., no HAZ or EN82H cracking).

(6) SCC initiation and failure occurred in the HAZ.

(7) Time-to-initiation not available because of noise associated with the EPD system due to room temperature air conditioner problems.

(8) This value could be ~40 mV more positive because of specimen polarization.

(9) Approximately 30 surface cracks were observed on one side of the HAZ in the Alloy 600.

(10) Multiple surface cracks were observed in the Alloy 600 regions, and 2 surface cracks were observed in the HAZ regions.

(11) Two cracks were observed in the Alloy 600 regions, and 2 surface cracks were observed in the HAZ regions.

Effect of Coolant Hydrogen

Figure 5 summarizes the SCC initiation time as a function of coolant hydrogen. Since the SCC cracks in all of the first five specimens tested occurred in the Alloy 600 regions for these specimens, the SCC initiation time data actually represents Alloy 600 heat NX5805G behavior. The five blue diamond data points represent Alloy 600 data from the HAZ specimen tests. The two green circles represent the data points for the HAZ specimens in which the SCC occurred in the HAZ region. Note that the initiation time for the specimen that initiated in the HAZ region is consistent with the results for the specimens in which the cracks occurred in the wrought material. Also included in Figure 5 are previously published results for tests conducted on mill-annealed (MA) Alloy 600 active-load test specimens for heat NX5805G indicated by the red squares [11].

Figure 5 illustrates that for the HAZ specimens the SCC initiation time is lengthened by a factor of ~2 as the coolant hydrogen concentration is increased from 30 to 75 cc/kg and by a factor of ~5 as the coolant hydrogen level is reduced from 30 to 1 cc/kg hydrogen at 360°C. In contrast, no discernible SCC initiation performance difference was noted between MA Alloy 600 specimens tested at coolant hydrogen levels of 30 and 75 cc/kg.

Figure 5 also includes a model prediction. This model is essentially the previously published coolant hydrogen SCC growth rate model [16]. Specifically, it was assumed that the SCC initiation and crack growth rate coolant hydrogen functionalities are equivalent. That is, if a 2X increase in the crack growth rate susceptibility occurred for a given change in ΔEcP (hydrogen level) this same increase in susceptibility would be associated with SCC initiation (2X decrease in initiation time). As illustrated in Figure 5 the model does a reasonable job in describing the observed SCC initiation coolant hydrogen response. A modest increase in SCC susceptibility is predicted when the hydrogen level is decreased from 75 to 30 cc/kg (1.1X), which is relatively consistent with the experimental data (HAZ specimens showed a 2X increase in SCC initiation susceptibility and no effect was observed with the mill-annealed specimens). An appreciable reduction in SCC susceptibility of 3x was predicted when the coolant hydrogen level is reduced from 30 to 1 cc/kg and a 5x reduction was observed in the HAZ specimens.

These coolant hydrogen initiation test results suggest that the SCC initiation and SCC growth (SCCGR) rate coolant hydrogen dependencies may be quantitatively similar. These SCCI coolant hydrogen results are also consistent with commercial U-bend SCCI tests which have shown that the SCCI and SCCGR coolant hydrogen effects are similar [17], Figure 6.

DISCUSSION

The lack of SCC within the HAZ regions was surprising in light of HAZ crack growth rate studies, which indicate a significant increase in the SCC crack growth rate susceptibility within the HAZ compared to the base metal, as shown in Figure 7 [1, 2]. Figure 7 summarizes tests conducted on an Alloy 600 HAZ fabricated by depositing EN82H filler metal onto a mill-annealed Alloy 600 plate via gas tungsten arc welding. Fracture mechanics based, stress corrosion crack growth rate testing was performed in high purity water between 315°C and 360°C at an initial stress intensity factor of 44 MPa$\sqrt{m}$. The HAZ samples exhibited significant SCC entirely within the HAZ at all temperatures tested and the crack growth rates were ~30X faster than the Alloy 600 base material tested at the same conditions.

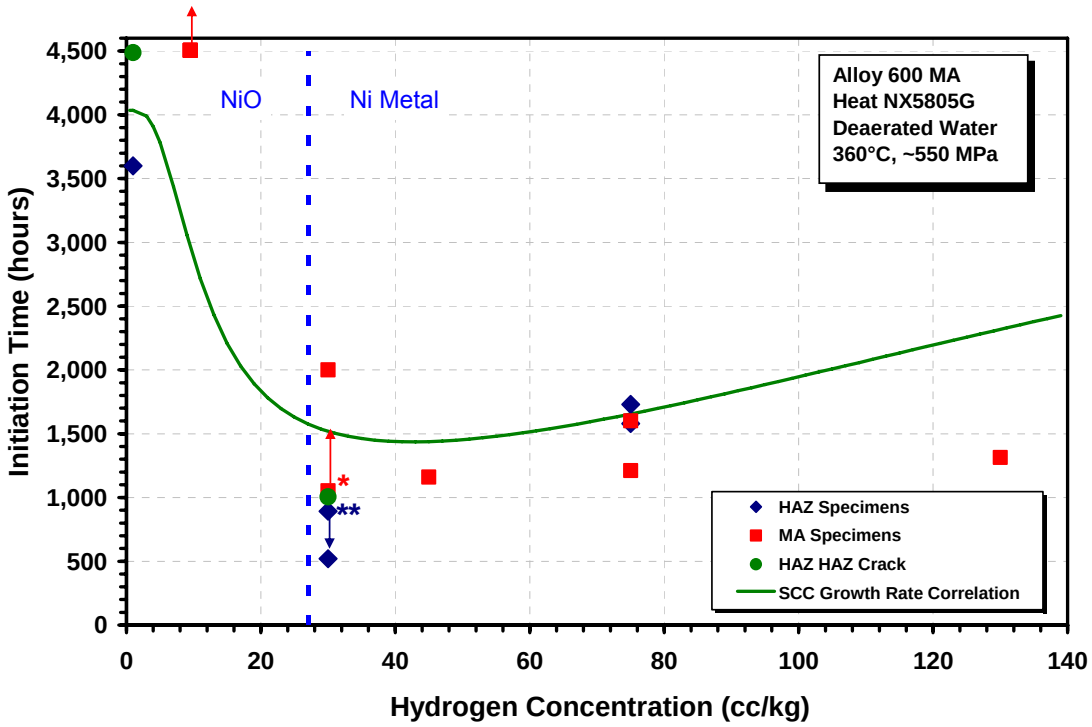

* Two small cracks observed after tensile pull, not detected by EPD (time represents exposure time)

** Multiple cracks observed prior to tensile pull, not detected by EPD (time represents exposure time)

Figure 5: Effect of coolant hydrogen on Alloy 600 SCC initiation in deaerated primary water at 360°C. Up arrows reflect specimens that did not SCC. Down arrows reflect specimen SCC occurred upon this exposure.

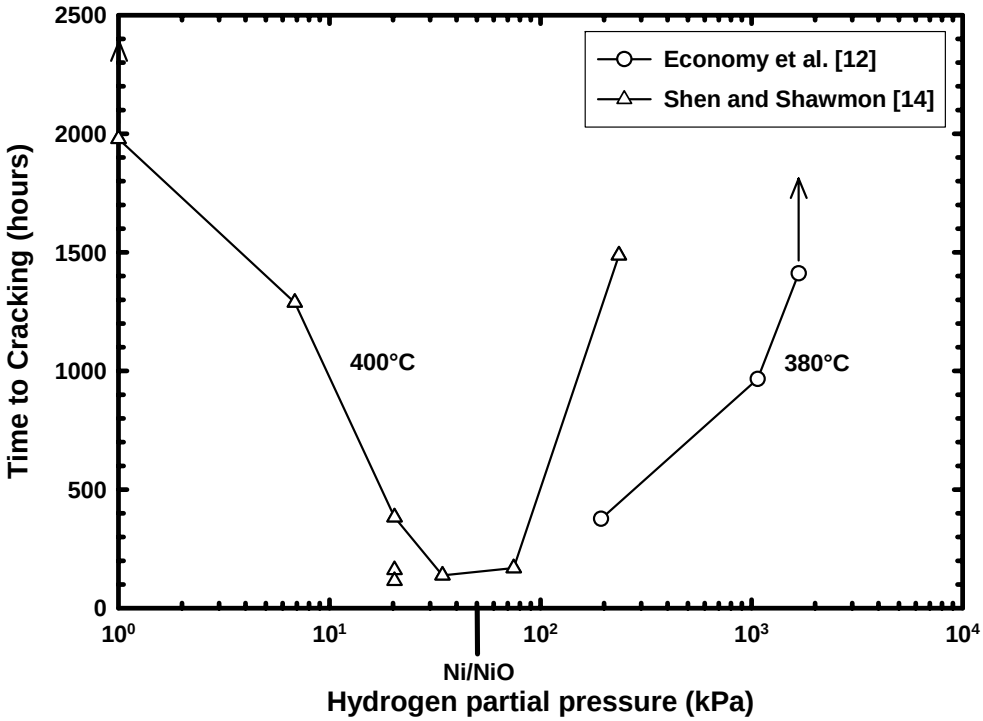

Figure 6: Effect of coolant hydrogen on Alloy 600 SCCI observed in commercial U-bend tests in steam [17].

It was previously hypothesized that the unexpected initiation results may be due to differences in the strain levels [11]. Specifically, the yield strength of the weld metal and HAZ regions of the narrow groove weld "HAZ" specimens is greater than the yield strength of the Alloy 600 region. Because of this yield strength difference, the Alloy 600 regions are expected to strain to a greater extent than the HAZ and weld metal regions when the HAZ specimens are loaded to a constant stress. Additionally, as detilaed later, prior SCC initiation tests conducted on wrought Alloy 600 suggested that initiation time correlated better with bulk plastic strain than with stress [11]. This is consistent with the results of specimen GX8-28, which did contain a crack in the HAZ region. This specimen was pre-strained prior to testing to a slightly lower load than the test load. This pre-straining may have resulted in work hardening of the EN82H and Alloy 600 samples to different degrees (*i.e.* pre-straining likely resulted in similar yield strengths for the various regions after the initial loading). The EN82H and Alloy 600 regions may have been strained to similar levels during the test. As a result, microstructural differences would become more important than differences in plastic strain, thus the HAZ region (which microstructurally should be more susceptible) would crack.

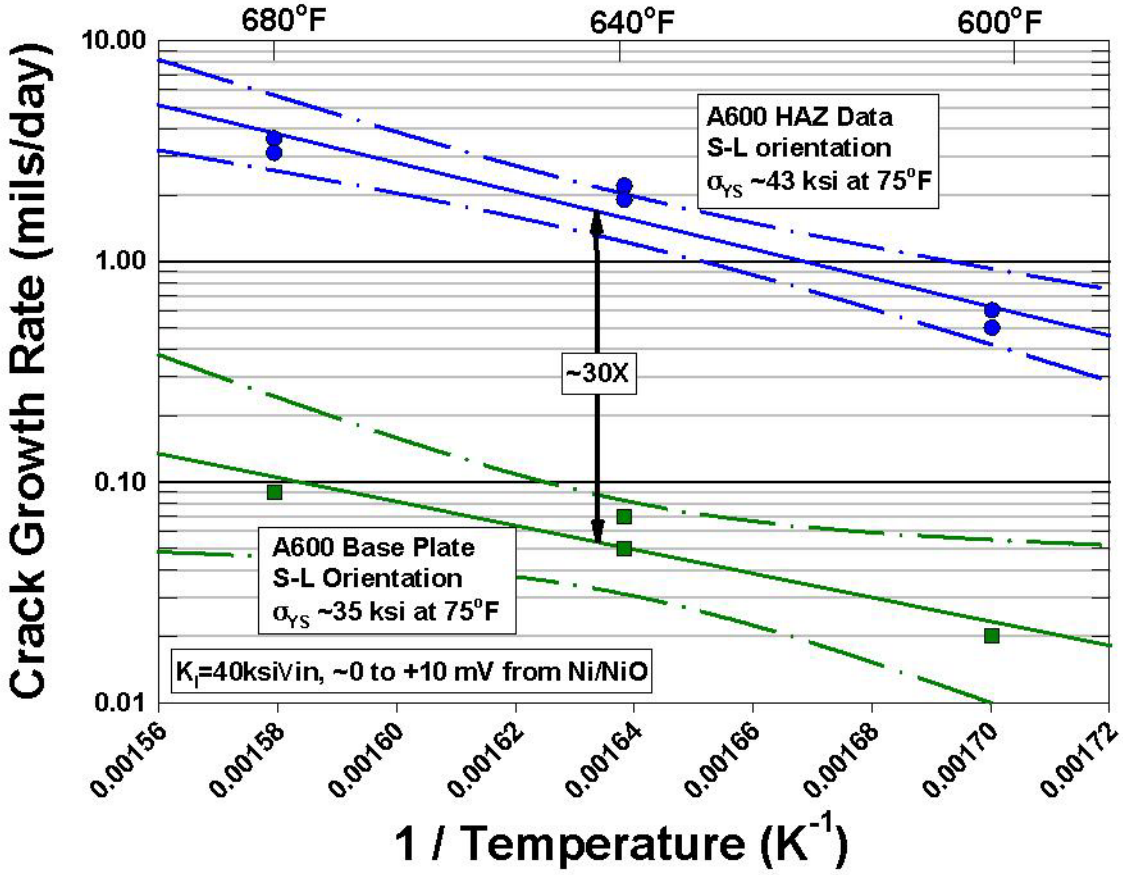

Figure 7: Comparison of the A600 HAZ data (blue points) with a prediction for typical high temperature annealed Alloy 600 (*i.e.*, the unaffected base material) [1].

In order to confirm this hypothesis, speckle image photogrammetry strain measurements were performed on a specimen to characterize the level of strain in each region. The specimen was subjected to the loading history shown in Figure 8. Figure 8 shows the load and crosshead displacement as a function of time. The specimen was initially loaded to 11.3 kN (2546 lbs) at a constant crosshead displacement rate. The sample was then unloaded in displacement control to 0.44 kN (100 lbs). Next, the sample was reloaded in displacement control to failure, although measurements were only performed up to a crosshead displacement of 12.7 mm (0.50 inches). Figure

9 shows the measurements of Von Mises strain at various points throughout the loading history. It was hypothesized that the differences in initiation response between the non-prestrained and prestrained HAZ specimens were due to differences in plastic strain in the HAZ region [11]. However, the Von Mises strain was consistently highest in the weld region, and differences were not observed between the Alloy 600 and HAZ regions before and after the unloading cycle. Thus, these results do not support this hypothesis.

The fact that SCC initiation did not occur in the weld metal region of the HAZ specimen even though the weld metal region experienced the highest surface strain is consistent with the results for samples consisting solely of weld metal [11]. SCC initiation has not been observed in EN82H specimens loaded to ~30% tensile strain at 680°F and 30 cc/kg H_2 after greater than 4000 hours. In comparison, Alloy 600 in the HTA and LTA conditions exhibited SCC initiation after ~1000 hours. Additionally, initiation has not been observed in the weld metal regions of the HAZ specimens, even though the speckled image photogrammetry results show that the weld region has the highest strain. These results suggest that under the same environmental conditions and strain level, EN82H is significantly more resistant to SCC initiation than Alloy 600. The lack of initiation in the EN82H specimens also suggests that SCC growth in weld metal must begin from a pre-existing weld defect, mechanical fatigue crack or corrosion fatigue crack. Figure 10 shows the SCC initiation time as a function of plastic strain for Alloy 600 and EN82H in deaerated water at 360°C. Results are shown for Alloy 600 in the mill annealed (MA), low temperature annealed (LTA), and high temperature annealed (HTA) conditions. Figure 10 includes prior results [11], as well as additional data for EN82H and LTA Alloy 600. As seen in Figure 10, the time to initiation decreases as the plastic strain increases. Included in Figure 10 are the results from two specimens of mill annealed Alloy 600 that were cold worked 12%. For the cold worked specimens, the data are shown at two locations, the plastic strain applied during loading, as well as the total plastic strain imparted to the sample during both cold rolling and loading. The data for cold rolled Alloy 600 suggests that the plastic strain imparted to the sample prior to loading the sample is important.

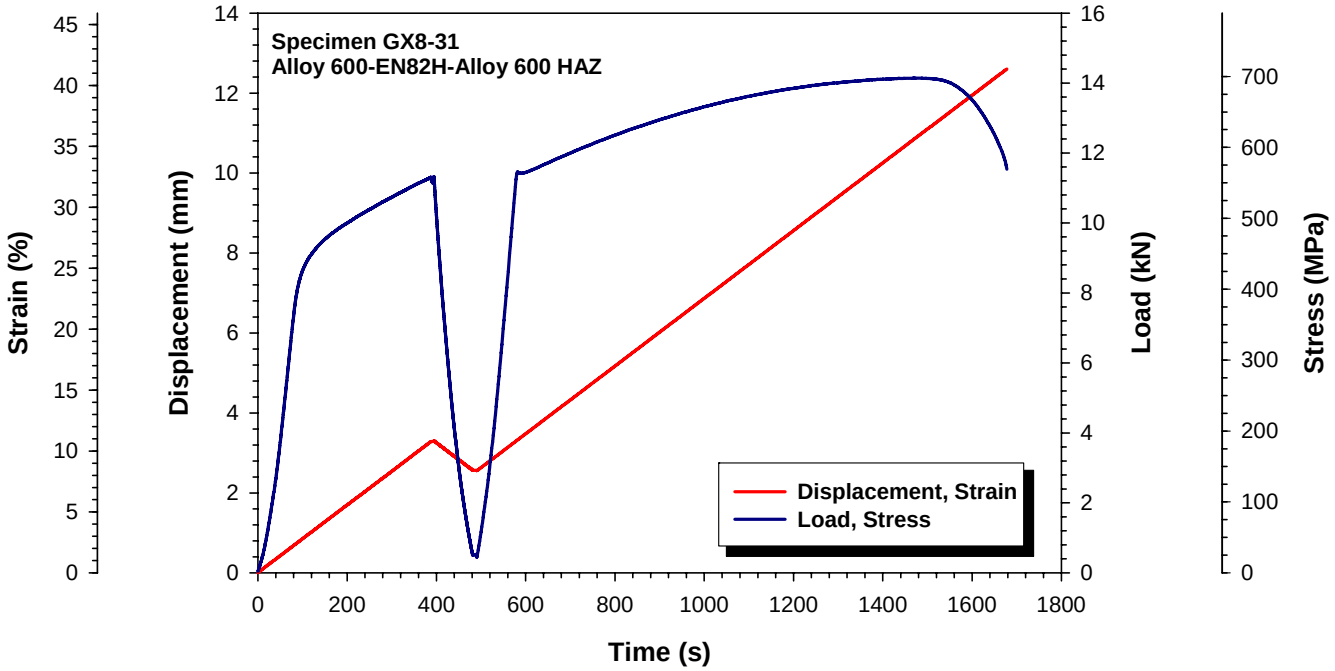

Figure 8: Crosshead displacement, load, engineering stress, and engineering strain as a function of time for HAZ specimen GX8-31 that was utilized for speckled image photogrammetry measurements

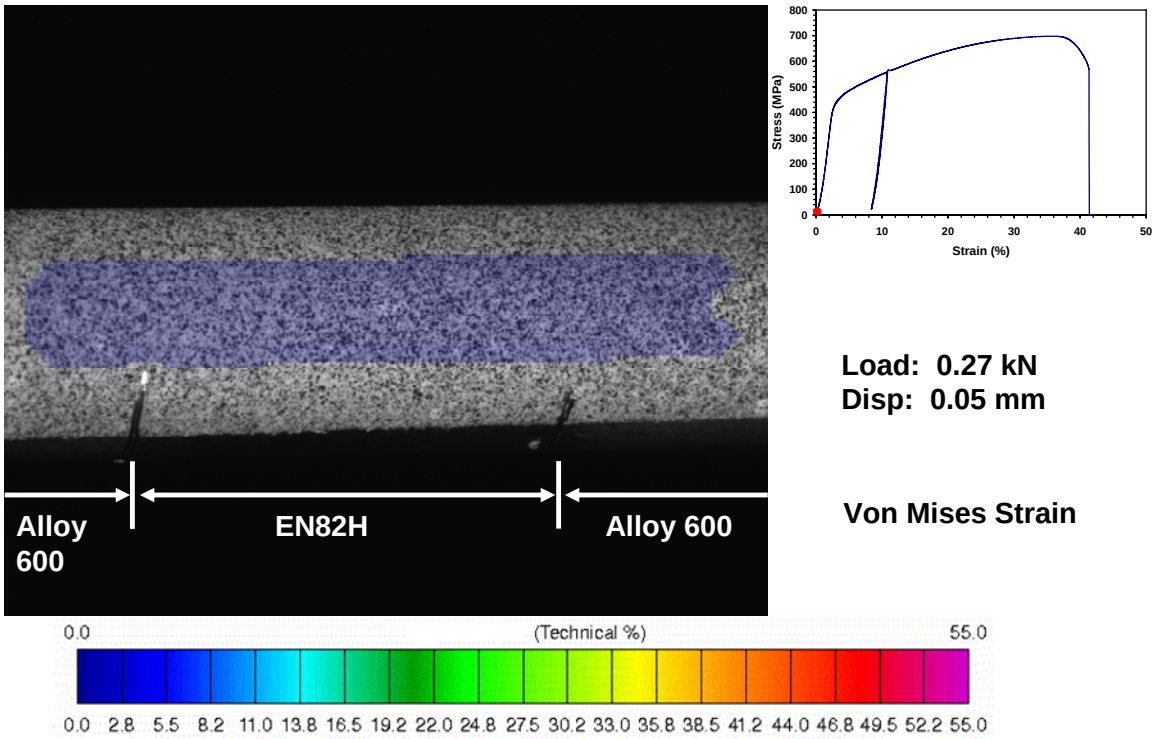

(a)

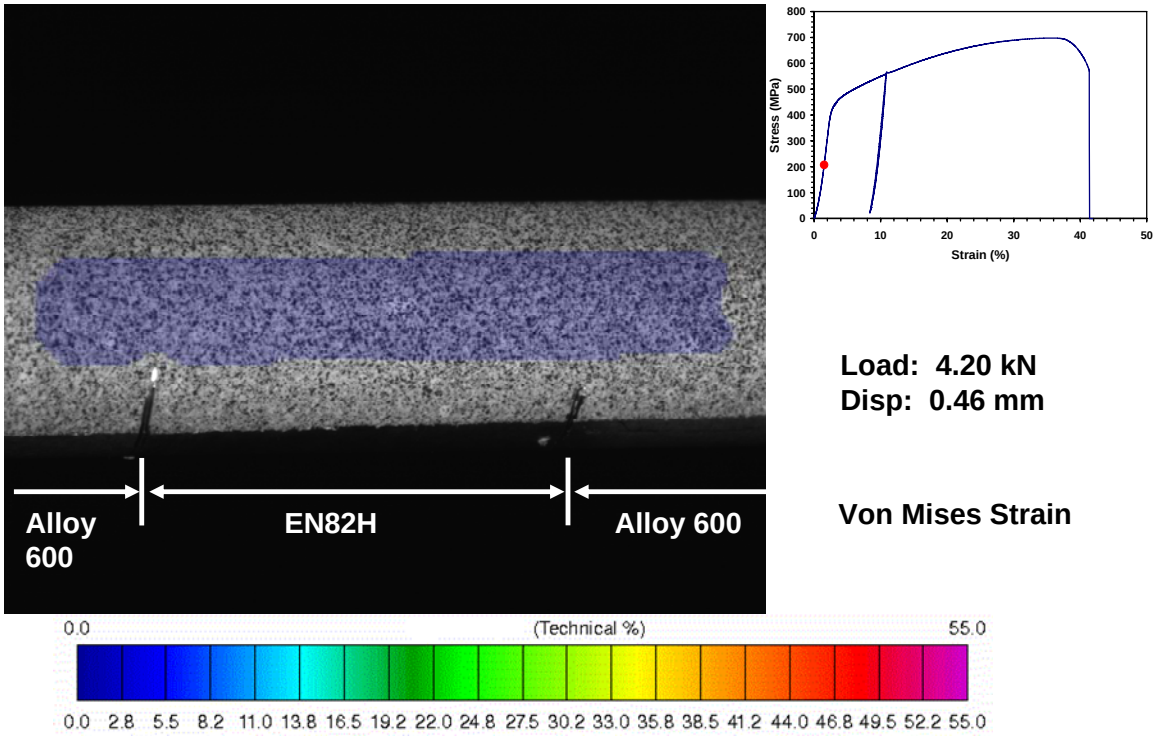

(b)

Figure 9: Speckled image photogrammetry measurement of the Von Mises strain in a HAZ test specimen loaded to (a) 0.27 kN and (b) 4.20 kN.

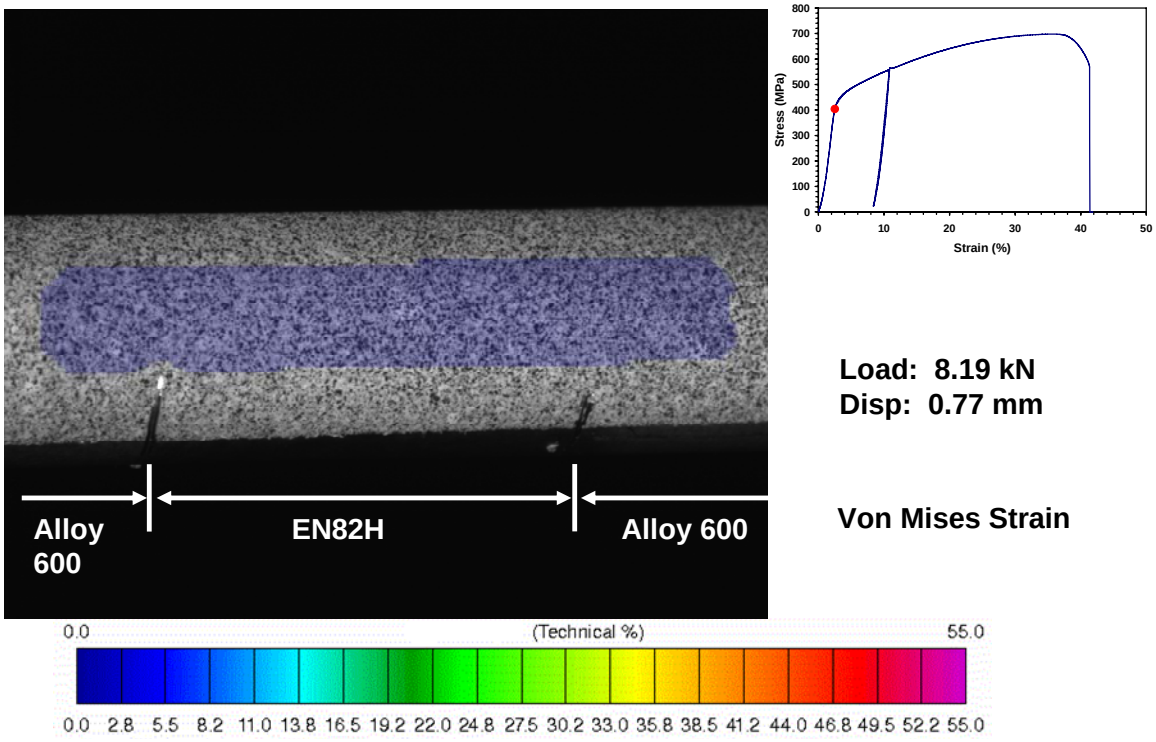

(c)

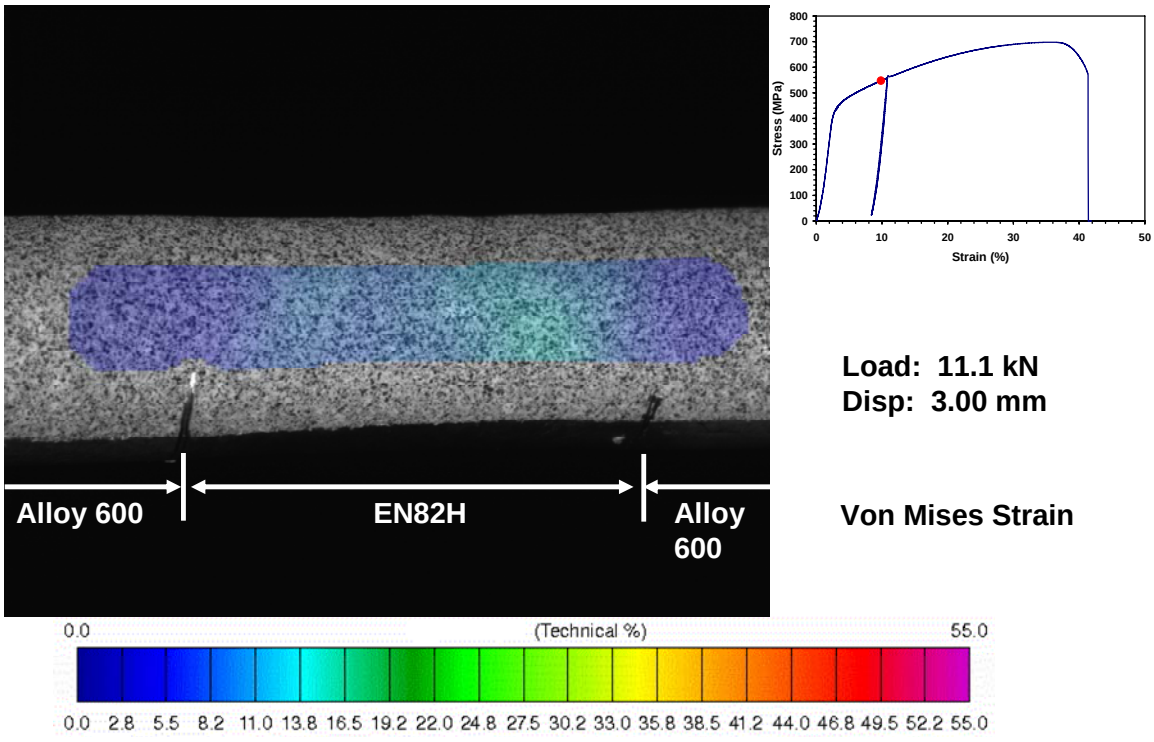

(d)

Figure 9: Speckled image photogrammetry measurement of the Von Mises strain in a HAZ test specimen loaded to (c) 8.19 kN and (d) 11.1 kN.

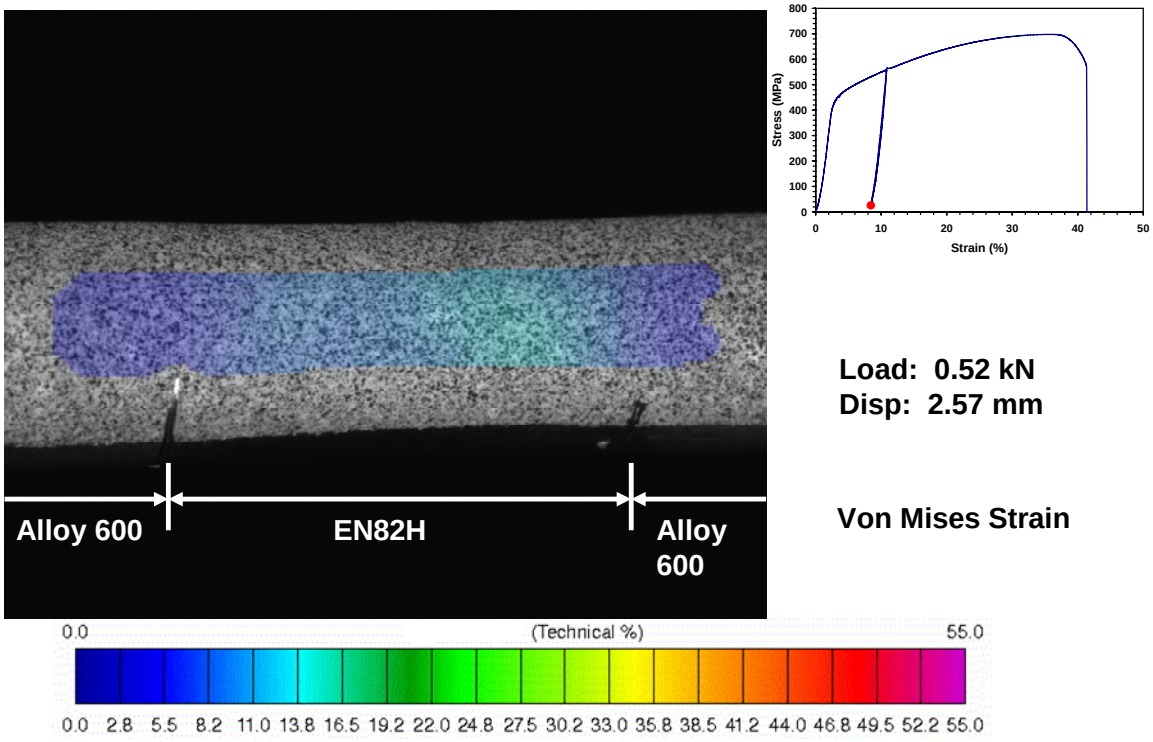

(e)

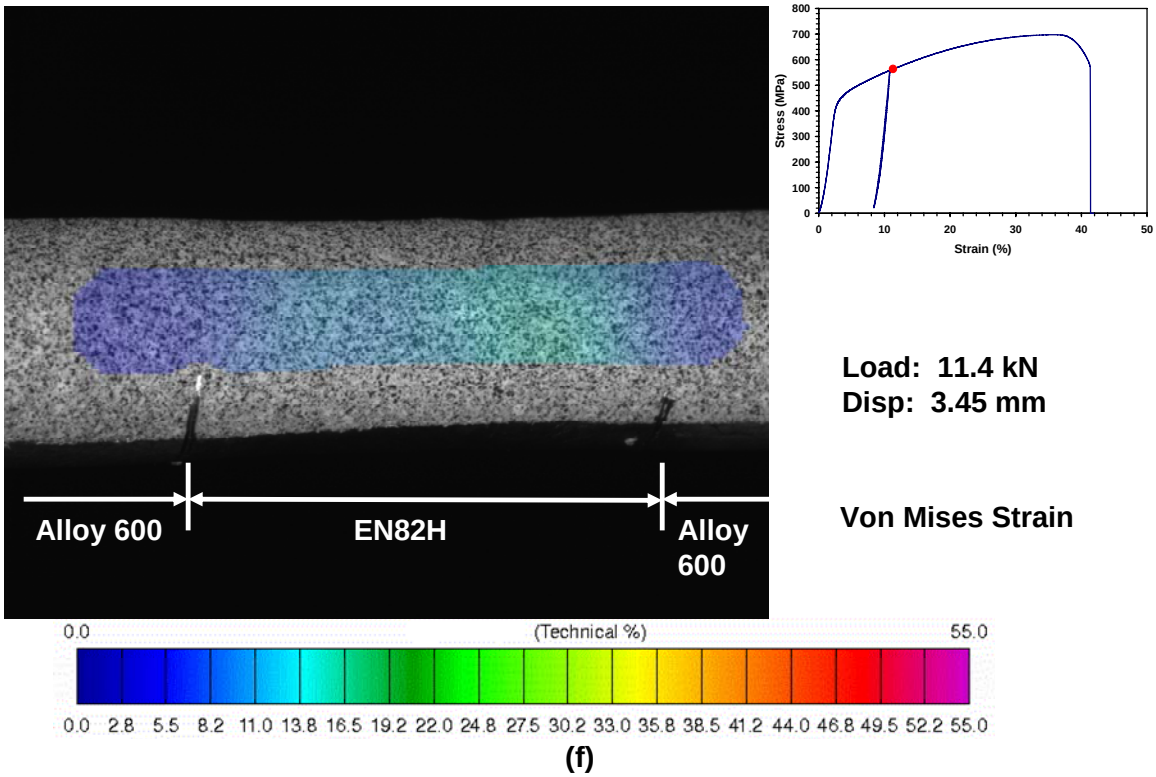

(f)

Figure 9: Speckled image photogrammetry measurement of the Von Mises strain in a HAZ test specimen loaded to (e) 0.52 kN and (f) 11.4 kN.

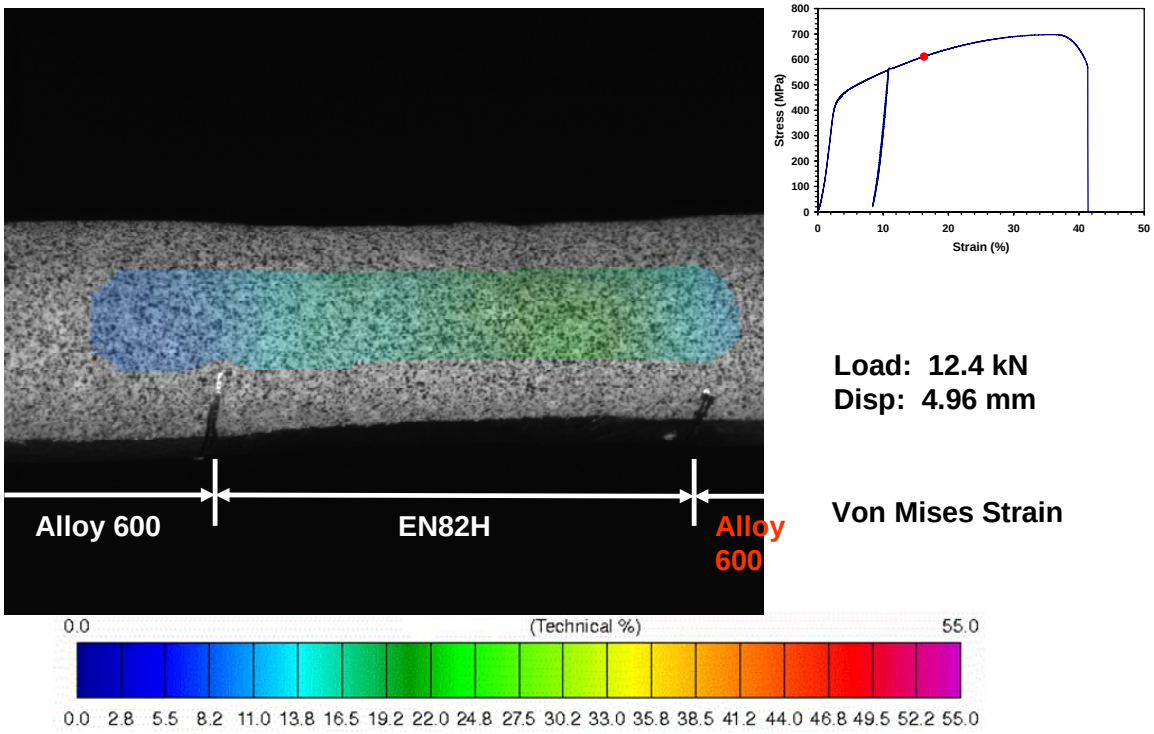

(g)

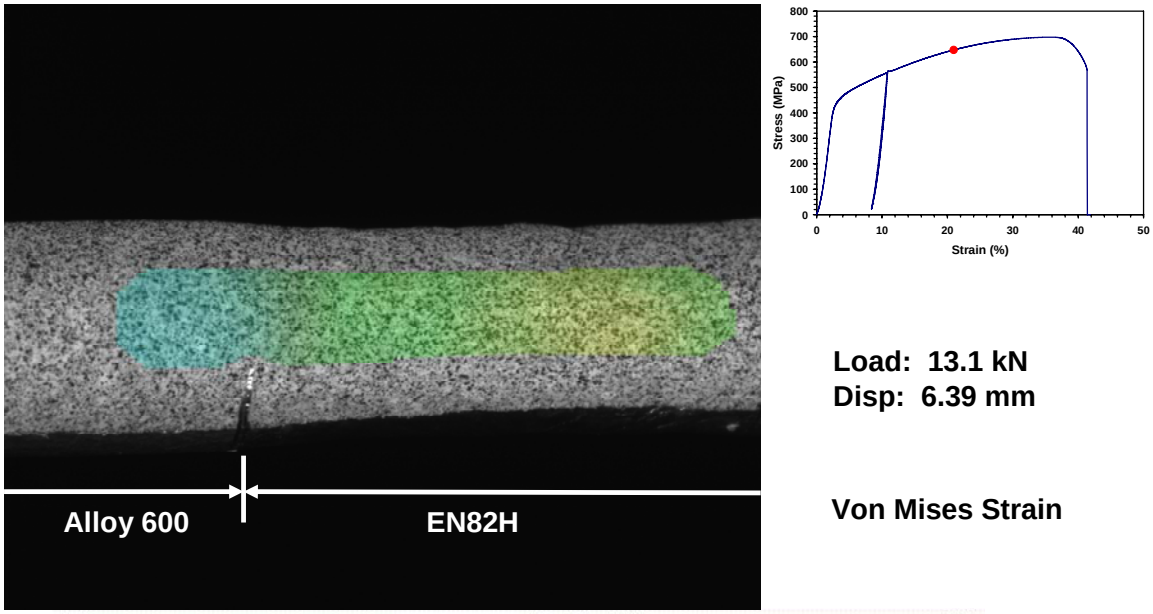

(h)

Figure 9: Speckled image photogrammetry measurement of the Von Mises strain in a HAZ test specimen loaded to (g) 12.4 kN and (h) 13.1 kN.

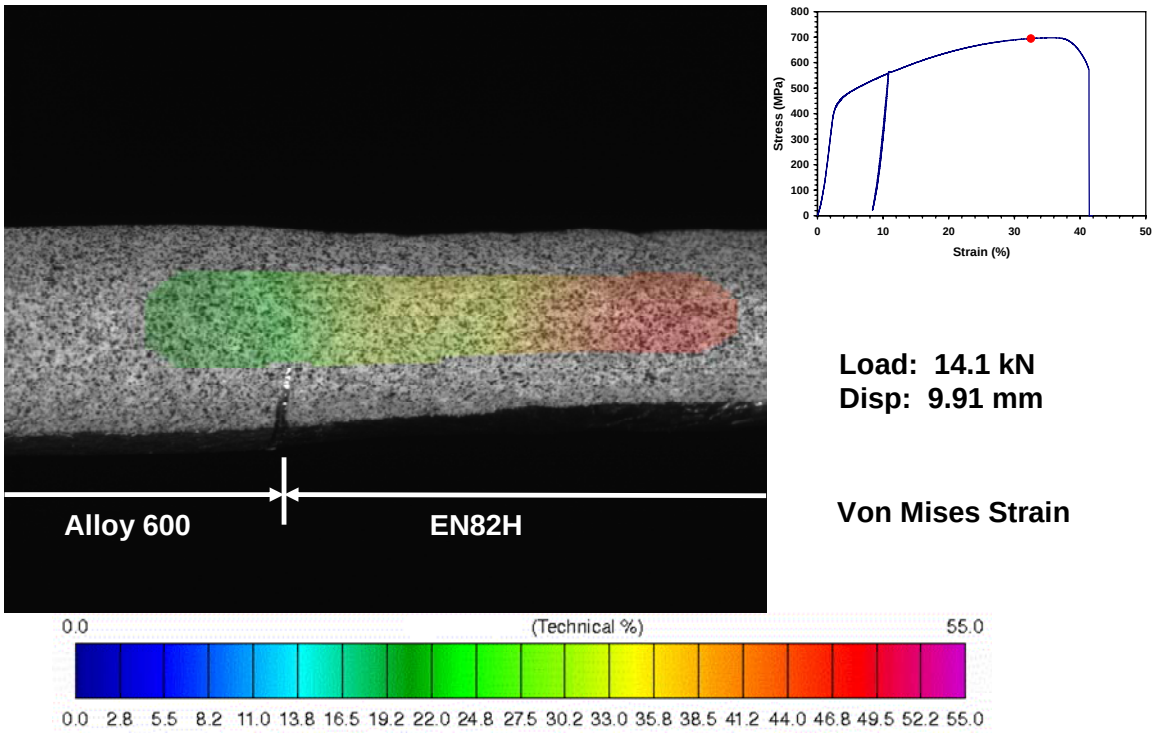

(i)

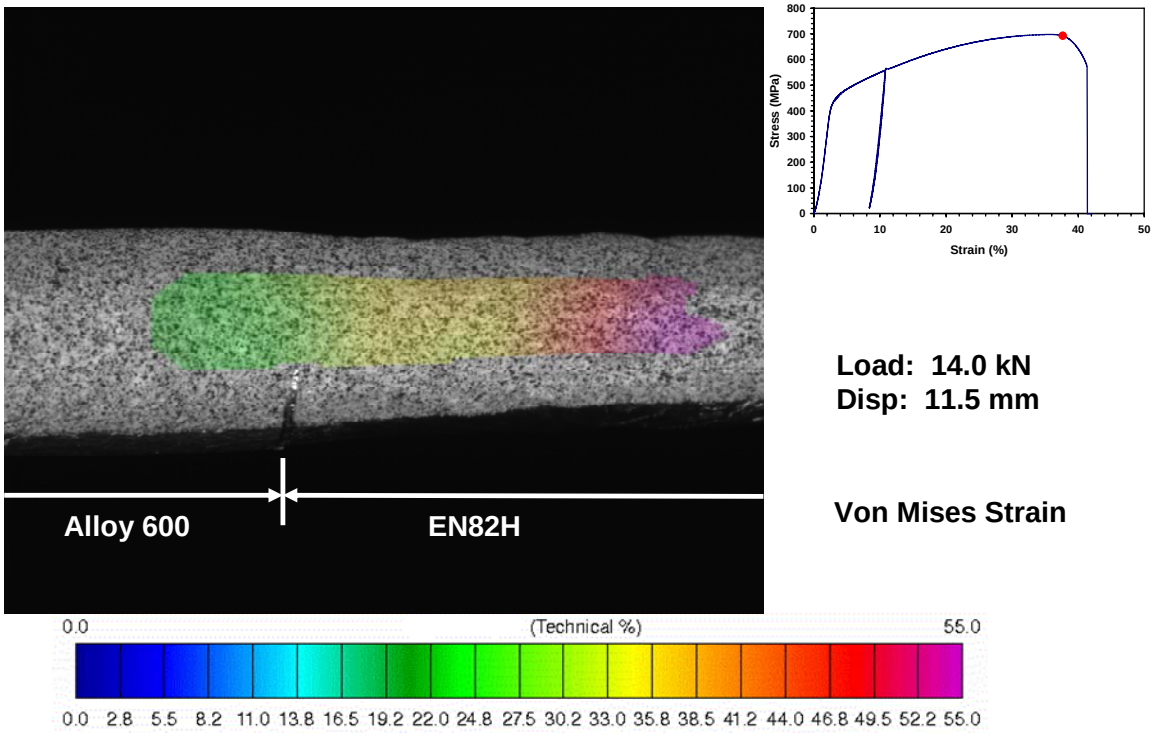

(j)

Figure 9: Speckled image photogrammetry measurement of the Von Mises strain in a HAZ test specimen loaded to (i) 14.1 kN and (j) 14.0 kN.

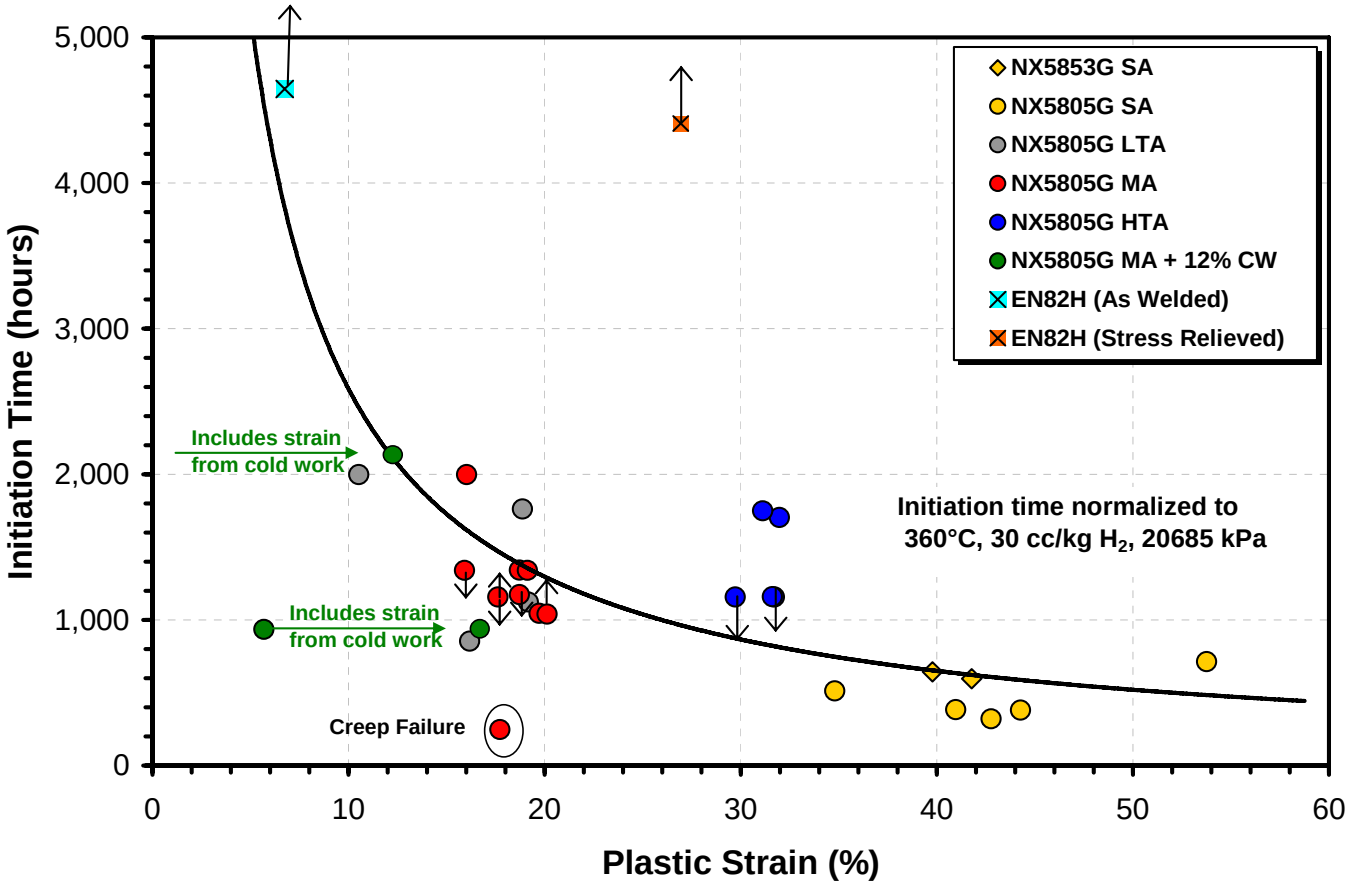

Figure 10: SCC initiation time as a function of plastic strain for Alloy 600 and EN82H in deaerated water at 360°C. Up arrows reflect specimens that did not initiate SCC [11]. Down arrows reflect specimens in which SCC occurred, but EPD was not able to detect initiation due to noise in the EPD response. For specimens with down arrows, the indicated time corresponds to the exposure time. All other SCC initiation times were determined by EPD.

Residual stress measurements were made using x-ray diffraction on an EN82H /Alloy 600 HAZ specimen in order to determine if the observed behavior was due to differences in surface residual tress between the various regions of the specimen. Measurements were made in the HAZ and in the wrought region. The diffraction patterns were collected with an area detector and calculations were based on the relationship between the stress tensor and the observed distortion in the diffraction cones. The pattern generated from the (220) planes using Cr K-α radiation were used for the measurements. A small size x-ray beam approximately 0.3 mm in diameter was used. Table 3 summarizes the calculated residual stresses and 1 standard deviation. Residual stress measurements suggest that the surface stresses are higher in the HAZ region than in the Alloy 600 wrought region.

Table 3: Residual Stresses in Alloy 600/EN82H HAZ Specimens

Region	Longitudinal Stress (MPa)	Shear Stress (MPa)	Transverse Stress (MPa)
HAZ	563.3 $\pm$ 55.2	-37.9 $\pm$ 40.7	224.8 $\pm$ 40.7
Wrought	448.2 $\pm$ 34.5	1.4 $\pm$ 30.3	75.9 $\pm$ 32.4

Table 4 summarizes additional possible explanations for the observed behavior in the HAZ specimens. The observed behavior for the HAZ specimens is likely not related to differences in the environment, differences in stress/strain between the various specimen regions, differences in surface residual stress, or differences in the grain boundary microstructure of the various specimen regions. The behavior may be related to differences in the intragranular microstructure and creep resistance of the various weld regions, differences in the oxide film stability for the various weld regions, or differences in the surface area of the various materials exposed to water.

Since it is possible that the observed behavior is related to the surface area of the various materials (weld, HAZ, wrought) exposed to high temperature water, work is in progress to fabricate a bulk HAZ sample via Gleeble methods. A range of thermal cycles with different peak temperatures, hold times at the peak temperature, and cooling rates are being applied to Alloy 600 test specimens to generate a bulk HAZ specimen with a microstructure consistent with the HAZ material test during prior SCC growth rate studies [1, 2].

CONCLUSIONS

- Test results suggest that the SCC initiation resistance of Alloy 600 and its weld metal follows the following order: EN82H > Alloy 600 HAZ > Alloy 600. The high SCC initiation resistance observed to date in Alloy 600 heat affected zones compared to wrought Alloy 600 is unexpected based on the microstructure of HAZ versus wrought material and based on prior SCC growth rate studies. The observed behavior for the HAZ specimens is likely not related to differences in the environment, differences in stress/strain between the various specimen regions, differences in surface residual stress, or differences in the grain boundary microstructure of the various specimen regions (weld, HAZ, wrought). The behavior may be related to differences in the intragranular microstructure and creep resistance of the various weld regions or differences in the surface area of the various materials (weld, HAZ< wrought) exposed to high temperature water.
- Speckled image photogrammetry results indicate that the highest Von Mises strain is within the weld metal region of the composite HAZ specimen, with significantly less strain in the Alloy 600 and HAZ regions. These results suggest that the lack of cracking in the HAZ region is not related to differences in stress/strain between the various specimen regions.
- Testing suggests that SCC initiation and SCC growth exhibit similar sensitivities to dissolved hydrogen.
- Preliminary results suggest that bulk plastic strain may be a better mechanical parameter than stress to characterize SCC initiation time in Alloy 600 exposed to high temperature, high purity water. However, limited testing of Alloy 600-EN82H-Alloy 600 HAZ specimens suggest that loading history also influences SCC initiation behavior.

Table 4: Summary of Possible Explanations for Observed Behavior in HAZ Specimens

Parameter	Observations	Discussion
Coolant Hydrogen Temperature	Alloy 600, EN82H, and HAZ regions in the HAZ specimens were exposed to the same environment within the autoclave.	Differences in environment likely not the cause
Stress/Strain	Alloy 600, EN82H, and HAZ regions in the HAZ specimens were loaded to the same stress. Speckled image photogrammetry results indicate highest surface strain is within the weld metal region, significantly less strain in the Alloy 600 and HAZ regions	Differences in stress or strain between the various specimen regions likely not the cause
Grain Boundary Microstructure	SCC growth rate studies indicate that Alloy HAZ material is more susceptible than EN82H and Alloy 600. SCC growth rates follow the following trend when samples are exposed to the same environmental and loading conditions: Alloy 600 HAZ > EN82H > Alloy 600	Differences in grain boundary microstructure between the various specimen regions likely not the cause
Surface Residual Stress	Residual stress measurements using X-ray diffraction suggest that the surface stresses are higher in the HAZ region than in the Alloy 600 wrought region.	Differences in surface residual stress likely not the cause.
Intragranular microstructure and creep resistance	Creep rate should be higher in the Alloy 600 region than in the EN82H region; creep rate of HAZ region is likely in between the creep rate for the wrought and weld region. Higher creep rate in Alloy 600 region may enhance SCC initiation susceptibility in pre-strained specimens.	Differences in Intragranular microstructure and creep resistance may be the cause
Surface area (volume) of Material Tested	SCC initiation is a stochastic process; likelihood of initiating SCC may be affected by surface area of material under load and exposed to the environment. HAZ specimens expose large amount of Alloy 600 and EN82H to the environment, but only small surface area of HAZ material.	Differences in surface area of material may be the cause
Oxide Film Stability	Oxide film may be more stable for EN82H due to higher Cr content (EN82H ~ 20% Cr, Alloy 600 ~ 15% Cr)	Differences in oxide film stability may be the cause

REFERENCES

1. GA Young, N Lewis, and DS Morton, "The Stress Corrosion Crack Growth Rate of Alloy 600 Heat Affected Zones Exposed to High Purity Water," in *USNRC-ANL Conference on Vessel Head Penetration Inspection, Cracking, and Repairs*, Gaithersburg, MD, Nuclear Regulatory Commission, 2003.
2. GA Young, et al., "The Mechanism and Modeling of Intergranular Stress Corrosion Cracking Of Nickel-Chromium-Iron Alloys Exposed To High Purity Water," in *Proceedings of the Twelfth International Conference on Environmental Degradation of Materials in Nuclear Power Systems - Water Reactors*, Salt Lake City, UT, American Nuclear Society, 2005.
3. GL Webb and MG Burke, "Stress Corrosion Cracking Behavior of Alloy 600 in High Temperature Water," in *Seventh International Symposium on Environmental Degradation of Materials in Nuclear Power Systems - Water Reactors*, Breckenridge, CO, NACE, 1995.
4. AF Gourgues, PM Scott, and E Andrieu, "A Study of the Mechanism of Primary Water Stress Corrosion Cracking of Alloy 600," in *Seventh International Symposium on Environmental Degradation of Materials in Nuclear Power Systems - Water Reactors*, Breckenridge, CO, NACE, 1995.
5. JK Sung, "Effect of Heat Treatment on Caustic Stress Corrosion Cracking Behavior of Alloy 600," *Corrosion*, Vol. 55, 1999, p. 1144-1154.
6. HA Domian, et al., "Effect of Microstructure on Stress Corrosion Cracking of Alloy 600 in High Purity Water," *Corrosion*, Vol. 33, 1977, p. 26-37.
7. RH Jones and SM Bruemmer, *Environment-Induced Crack Growth Processes in Nickel-Base Alloys*, in *Environment-Induced Cracking Of Metals*, R. Gangloff and M. Ives, Editors, National Association of Corrosion Engineers, 1988, p. 287-310.
8. GS Was, HH Tischner, and RM Latanision, "The Influence of Thermal Treatment on the Chemistry and Structure of Grain Boundaries in Inconel 600," *Metallurgical Transactions A*, Vol. 12A, 1981, p. 1397-1408.
9. G Economy, RJ Jacko, and FW Pement, "IGSCC Behavior of Alloy 600 Steam Generator Tubing in Water or Steam Tests Above 360 C," *Corrosion*, Vol. 43, 1987, p. 727-734.
10. GA Young, et al., "Quantification of Residual Plastic Strains in Ni-Cr-Mn-Nb GTAW Welds via Electron Backscatter Diffraction," in *Sixth International Conference on Trends in Welding Research*, Pine Mountain, GA, 2002.
11. E Richey, DS Morton, and MK Schurman, "SCC Initiation Testing of Nickel-Based Alloys Using In-Situ Monitored Uniaxial Tensile Specimens," in *Proceedings of the Twelfth International Conference on Environmental Degradation of Materials in Nuclear Power Systems - Water Reactors*, Salt Lake City, UT, American Nuclear Society, 2005.
12. SA Attanasio and DS Morton, "Measurement of the Nickel/Nickel Oxide Transition in Ni-Cr-Fe Alloys and Updated Data and Correlations to Quantify the Effect of Aqueous Hydrogen on Primary Water SCC," in *11th International Conference on Environmental Degradation of Materials in Nuclear Systems*, Stevenson, WA, National Association of Corrosion Engineers, 2003.
13. DS Morton, SA Attanasio, and GA Young, "Primary Water SCC Understanding and Characterization Through Fundamental Testing in the Vicinity of the Nickel / Nickel Oxide Phase Transition," in *Proceedings of the Tenth International Conference on Environmental Degradation of Materials in Nuclear Power Systems - Water Reactors*, Lake Tahoe, NV, National Association of Corrosion Engineers, 2001.
14. DS Morton, SA Attanasio, and GA Young, "Paper 01117, The Influence of Dissolved Hydrogen on Nickel Alloy SCC: A Window to Fundamental Insight," in *CORROSION / 2001*, Houston, TX, National Association of Corrosion Engineers, 2001.
15. DS Morton, et al., "In Search of the True Temperature and Stress Intensity Factor Dependencies of PWSCC," in *Proceedings of the Twelfth International Conference on Environmental Degradation of Materials in Nuclear Power Systems - Water Reactors*, Salt Lake City, UT, American Nuclear Society, 2005.

16. E Richey, DS Morton, and WC Moshier, "Paper 06513: Influence of Specimen Size on the SCC Growth Rate of Ni-Alloys Exposed to High Temperature Water," in *CORROSION / 2006*, San Diego, CA, National Association of Corrosion Engineers, 2006.
17. T Cassagne, et al., "An Update on the Influence of Hydrogen on the PWSCC of Nickel Base Alloys in High Temperature Water," in *Eighth International Symposium on Environmental Degradation of Materials in Nuclear Power Systems - Water Reactors*, Amelia Island, FL, American Nuclear Society, 1997.